



**HAL**  
open science

# Potential of an Embedded Hyperspectral Compressive Imaging System for Remote Sensing Applications

Olivier Lim, Stéphane Mancini, Mauro Dalla Mura

► **To cite this version:**

Olivier Lim, Stéphane Mancini, Mauro Dalla Mura. Potential of an Embedded Hyperspectral Compressive Imaging System for Remote Sensing Applications. IGARSS 2023 - 2023 IEEE International Geoscience and Remote Sensing Symposium, Jul 2023, Pasadena, United States. pp.4238-4241, 10.1109/IGARSS52108.2023.10282751 . hal-04281798v2

**HAL Id: hal-04281798**

**<https://hal.science/hal-04281798v2>**

Submitted on 24 Apr 2024

**HAL** is a multi-disciplinary open access archive for the deposit and dissemination of scientific research documents, whether they are published or not. The documents may come from teaching and research institutions in France or abroad, or from public or private research centers.

L'archive ouverte pluridisciplinaire **HAL**, est destinée au dépôt et à la diffusion de documents scientifiques de niveau recherche, publiés ou non, émanant des établissements d'enseignement et de recherche français ou étrangers, des laboratoires publics ou privés.

# POTENTIAL OF AN EMBEDDED HYPERSPECTRAL COMPRESSIVE IMAGING SYSTEM FOR REMOTE SENSING APPLICATIONS

Olivier Lim<sup>1,2</sup>, Stéphane Mancini<sup>1</sup>, Mauro Dalla Mura<sup>2,3</sup>

1. Univ. Grenoble Alpes, CNRS, Grenoble INP, TIMA, 46 avenue Félix Viallet 38031 Grenoble Cedex, France

2. Univ. Grenoble Alpes, CNRS, Grenoble INP, GIPSA-lab, 11 rue des Mathématiques 38402 Saint Martin d'Hères, France

3. Institut Universitaire de France (IUF), 1 rue Descartes 75231 Paris Cedex 05, France

## ABSTRACT

The utilization of hyperspectral imaging in remote sensing has seen an increasing trend, as it enables to capture a greater amount of information. In this context, emerging snapshot sensors based on compressed sensing have been employed for various remote sensing applications. This work presents a prospective study by proposing a method to evaluate the performances we can expect when reconstructing data from a compressed sensing imager, the Double-Disperser Coded Aperture Snapshot Spectral Imager on an embedded system, i.e. on either a Graphics Processing Unit or a Field-Programmable Gate Arrays. This is original in the literature since most compressive sensing works focus on reconstruction quality and overlook the requirements for real-time, namely computational cost and data bandwidth. Moreover, works that use an embedded system are even more scarce. The study introduces methods to enhance these restrictions and assesses the resulting improvements. The study's findings support the use of Disperser Coded Aperture Snapshot Spectral Imager for remote sensing applications, potentially enabling a smaller sensor size.

**Index Terms**— Compressed sensing, CGNE, DD CASSI, hyperspectral imaging, computation complexity, embedded systems, FPGA, GPU

## 1. INTRODUCTION

Hyperspectral imaging (HSI) is increasingly used in remote sensing (e.g. vegetation monitoring, hydrology, geology, ...) [1, 2]. The majority of sensors used in HSI and, more commonly in optical remote sensing for Earth observation from satellite or airborne platforms, are based on a scanning mechanism (e.g. pushbroom sensors) [3]. Alternative instruments exist and start to be used in remote sensing, for instance snapshot sensors such as the the pushframe cameras used by Planet satellites [4]. Snapshot sensors have been proposed recently [5] to perform HSI. Among them, we take a closer look at Compressed Sensing (CS) [6] based sensors such as the Coded Aperture Snapshot Spectral Imager (CASSI) [7], the *Double-Disperser Coded Aperture Snapshot Spectral*

*Imager* (DD CASSI) [8] or the *the Dual-Camera Compressive Hyperspectral Imager* (DCCHI) [9]. Thanks to CS, it is possible to capture hyperspectral data, as a data cube, from a single acquisition of a 2D sensor array. In literature, we can find some works that exploit these sensors for remote sensing applications [10, 11, 12].

However, raw acquired data from these sensors usually requires a computational step in order to process it and reconstruct the hyperspectral scene. This can be done through optimization algorithms [13] and, more recently, Deep Learning [14]. These methods usually come with long execution time which is a limiting factor for image reconstruction on the platform (drone or satellite) for live decision making (e.g. monitoring activities, hazard tracking, ...). The image reconstruction operation can be sped up thanks to algorithmic and hardware accelerations, i.e. by implementing the algorithms on Graphics Processing Units (GPUs) or Field-Programmable Gate Arrays (FPGAs).

However, there exist very few works about hyperspectral reconstruction based on CS and embedded systems. Among those, we can mention [15] that proposes a Deep Learning approach by mixing U-net [16] and Generative Adversarial Network (GAN) [17] while using the CASSI. And [18] which uses the DCCHI with Two-Step Iterative Shrinkage/Thresholding (TWiST) [19] coupled with the Alternating Direction Method of Multipliers (ADMM) [20] for the reconstruction process. Both of these works use GPUs for their reconstruction process and we are not aware of any work that use FPGAs.

In this paper we want to assess the potential of an embedded hyperspectral compressive imaging system for remote sensing applications while considering an embedded implementation, either on GPU or FPGA. This work proposes a study on feasibility and performance (regarding resolution and reconstruction quality) assessment of an imaging system based on coded aperture for hyperspectral remote sensing purposes. This study is based on a previous work [21] while taking into consideration that the acquisitions are performed from a flying platform which is a inherent to remote sensing acquisitions for Earth observation. Specifically, the reconstruction process is time-constrained and dependent on the

exposure time of the observed scene. This aspect is crucial for enabling online sensing applications.

## 2. METHODOLOGY

### 2.1. System description

For this study, we consider an imaging system made of the DD CASSI and the Conjugate Gradient for Normal Equation (CGNE) [22] as reconstruction algorithm. We made these choices because they are both well-known and we consider them as representative of, respectively, the CASSI class imagers and optimization algorithms.

We study a reconstruction approach proposed by Ardi et al. [23] and based on DD CASSI, CGNE and Tikhonov regularization. However, we consider a row-by-row reconstruction, similarly to a pushbroom imager. It is more appropriate for remote sensing and it helps reducing the size of the algorithm variables and, hence, their memory footprint. Which allows to reconstruct larger scenes before memory swapping<sup>1</sup> is needed.

To reconstruct the hyperspectral cube, the optimization problem to solve is formulated as follows:

$$\hat{\mathbf{o}} = \arg \min_{\mathbf{o}} \{ \|\mathbf{d} - \mathbf{H}\mathbf{o}\|^2 + \Omega(\mathbf{o}) \} \quad (1)$$

where  $\mathbf{d}$  is the data acquired by the DD CASSI,  $\mathbf{H}$  is the matrix representing the transfer function of the DD CASSI,  $\hat{\mathbf{o}}$  is the estimation of the observed scene  $\mathbf{o}$ ,  $\Omega(\mathbf{o}) = \mu_x \|\mathbf{D}_x \mathbf{o}\|^2 + \mu_\lambda \|\mathbf{D}_\lambda \mathbf{o}\|^2$  is a penalization function where  $\mathbf{D}_x$ , and  $\mathbf{D}_\lambda$  are the finite difference matrices along the spatial dimensions  $x$ ,  $y$  and the spectral dimension  $\lambda$  and  $\mu_x$ ,  $\mu_\lambda$  their respective regularization coefficients. Since the CGNE is used to solve problems of the form  $\mathbf{A}\mathbf{x} = \mathbf{b}$ , we denote  $\mathbf{A} = \mathbf{M}^\top \mathbf{M}$  and  $\mathbf{b} = \mathbf{H}^\top \mathbf{d}$  with  $\mathbf{M} = [\mathbf{H}, \sqrt{\mu_x} \mathbf{D}_x, \sqrt{\mu_\lambda} \mathbf{D}_\lambda]$ .

### 2.2. Complexity analysis

For a  $C \times W$  line (i.e.  $C$  columns and  $W$  wavelengths), the CGNE has a computational cost of  $2(CW)^2 + i(2(CW)^2 + 5CW)$  multiply-accumulate operations (MAC)<sup>2</sup>, with  $i$  the number of CGNE iterations. Regarding the memory footprint, it has to store  $(CW)^2 + 4CW + 3$  values. As an example, let us consider the case of the Airborne Visible/InfraRed Imaging Spectrometer (AVIRIS) project [24]. Solely with regards to computational cost, the amount of computations for a line is around  $3.5 \times 10^{15}$  MAC, considering  $i = CW/2$ , while current high end GPUs or FPGAs are able to perform around  $10^{12}$  MAC per second. The time taken for acquiring a  $677 \times 224$  line is about 100 ms. Given this timeframe, it is

<sup>1</sup>Memory swapping is used when the "work" memory is full during computations. Data in work memory is saved in external memory to be used later while needed data is loaded from an external memory.

<sup>2</sup>A MAC operation is the product of two variables added to an accumulator:  $a \leftarrow a + (b \times c)$ . GPUs and FPGAs are designed to perform this kind of arithmetical operations efficiently.

not feasible to reconstruct the line hyperspectral cube in these conditions and then real-time reconstruction is unachievable.

### 2.3. Proposed improvement strategies

To improve the reconstruction time, we studied two improvements. First, the use of a sparse matrix format. When looking closer at  $\mathbf{A}$ , we notice that it is made of diagonal patterns. We can determine that the maximum number of entries in  $\mathbf{A}$  is equal to  $E = (W + 2)CW - 2$ . For the example on AVIRIS, this represents a density of 1%. Using a sparse matrix format is beneficial in this case to reduce both the memory footprint and the computational cost when doing matrix-vector multiplications. Multiple sparse matrix formats exist, see [25]. Considering the entries pattern in  $\mathbf{A}$ , the Compressed Sparse Row (CSR) and Diagonal format (DIA) formats might be the most relevant. However, based on the experiment presented in Section 3, the CSR format yields the best results regarding reconstruction time. With this format,  $\mathbf{A}$  has a memory footprint of  $E \times (N_b + \lceil \log_2(CW) \rceil) + (CW + 1) \times \lceil \log_2(E) \rceil$  bits, where  $N_b$  denotes the number of bits used to represent an entry of  $\mathbf{A}$ . The computation cost of the improved CGNE is now  $2(CW^2 + 2CW - 2) + i \times [2CW^2 + 9CW - 4]$ .

The second improvement is related to the number representation format. By tuning it, we can reduce the memory footprint of the stored values and then the memory bandwidth. Additionally, on a hardware level, FPGAs can benefit from fixed-point representation. In this representation, a value has a fixed number  $e$  and  $v$  of bits to represent, respectively, the decimal and the fractional part. Compared to floating-point representation, fixed-point representation offers more freedom in setting the data size, consumes less power and requires fewer logic gates; but at a cost of a narrower representation range and lower precision. See [26] for more details. However, when altering the number representation, we have to consider the computational noise, that is, the accumulation of inaccuracy in computations that may lead to poor results. The simulations show that 64-bit floating-point (FP64), 32-bit floating-point (FP32), and fixed-point representations with  $v = \{32, 24\}$  offer a close reconstruction quality. And reconstruction quality decrease significantly for  $v = \{16, 12, 8\}$ .

Nonetheless, even with both improvements and considering the spatial resolution of AVIRIS, the required bandwidth to reconstruct the 224 spectral bands is still too high. We estimate that it would be possible to reconstruct up to 115 spectral bands while maintaining real-time reconstructions.

## 3. EXPERIMENTS

Experiments are made on scenes obtained from AVIRIS [24] and Reflective Optics System Imaging Spectrometer (ROSIS) [27] imagers. These scenes are depicted in Figure 1. Moreover, during the experiments, the CGNE's number of iterations is limited. This limit is defined so that the reconstruction

time does not exceed the exposure time of every line. This allows to assess the achieved quality in real-time conditions.

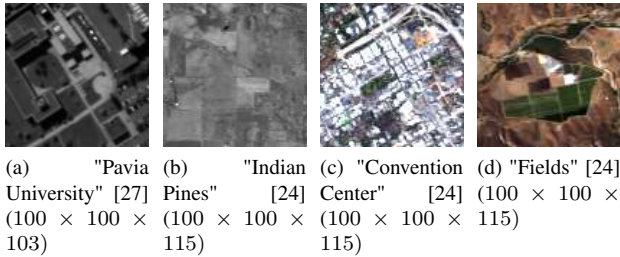


**Fig. 1:** Scenes used in the simulations with their dimensions and the original imager

### 3.1. Reconstruction time

Sparse matrix formats' improvement is evaluated by comparing the reconstruction times with the one measured with the default format. On top of the CSR and DIA formats, this comparison include the Block Sparse Row (BSR) et COOrdinate (COO). Reconstruction times are presented in Table 1. The CSR format offers the best improvement since it divides the reconstruction times by 34.85 in average. Regardless of the sparse matrix format, we can still notice that it improves the reconstruction time.

	Indian pines	Pavia University	Convention center	Fields
Default	1220.5	635.1	867.6	949.1
BSR	210.5 (5.8)	99.0 (6.4)	145.5 (6.0)	156.8 (6.1)
COO	103.0 (11.8)	54.1 (11.7)	73.0 (11.9)	79.5 (11.9)
CSR	<b>35.0 (34.9)</b>	<b>18.5 (34.4)</b>	<b>24.8 (35.0)</b>	<b>27.0 (35.1)</b>
DIA	263.1 (4.6)	131.9 (4.8)	186.3 (4.7)	204.5 (4.6)

**Table 1:** Average reconstruction times (in seconds) measured on a CPU. Speedup factors are given in parenthesis and best values in bold.

### 3.2. Computational noise

Regarding number representation, we performed simulations on FP64, FP32 and fixed-point with a varying number  $v$  of bits for the fractional part. In order to separate the computational noise from the CGNE reconstruction noise, reconstruction simulations are performed with an increasing number  $N$  of acquisitions and up to  $W$ , i.e. as many acquisitions of the scene as its spectral dimension. And, although the DD CASSI is a snapshot imager, increasing  $N$  allows to know whether performing multiple acquisitions is required in order to obtain a decent quality.

FP64 serves as the reference to compare the other number representations because it offers the highest precision among them. The reconstruction quality are measured by the Peak Signal-to-Noise Ratio (PSNR) and Structural Similarity Index (SSIM) and is depicted in Figure 2. We can say that FP64,

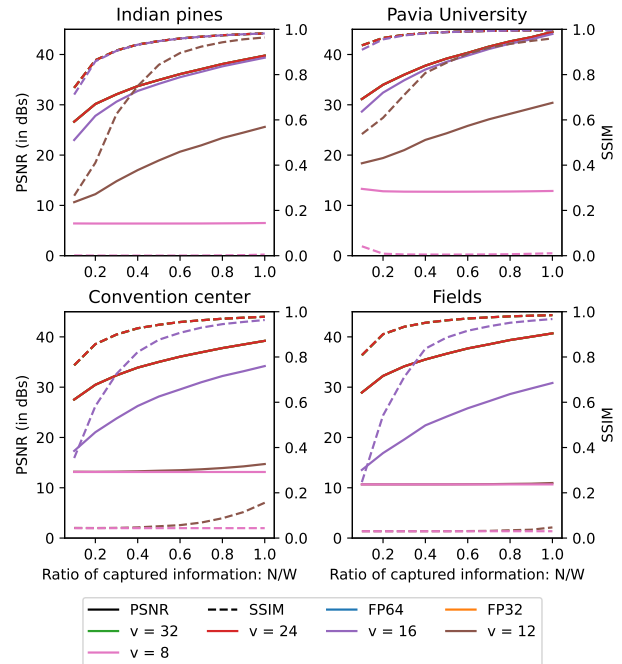


**Fig. 2:** Reconstruction quality depending on number representation.  $v$  denotes the number of bits of the fixed-point's fractional part.

FP32 and fixed-point representations with  $v = \{32, 24\}$  produce results with similar or close quality, since their curves overlap. However,  $v = \{16, 12, 8\}$  can convincingly be discarded as the quality deteriorates significantly. The resulting PSNR is between 15.75 and 44.49 dB, the SSIM is between 0.23 and 1.00. In order to reach a minimum threshold of 30 dB, about 20 acquisitions are required. We can nevertheless note that for Pavia University has a PSNR of 31.14 dB with 11 acquisitions.

## 4. CONCLUSION

The use of a compressed sensing imager, the DD CASSI, on embedded system for remote sensing applications is possible. Although the DD CASSI is a snapshot imager, we need to perform multiple acquisitions in order to get a satisfying quality. This is conceivable by using time delay integration [28], for instance. After determining the data transfers involved in the CGNE, we conclude that the data bandwidth of the computing devices allow hyperspectral reconstructions with up to 115 spectral bands for AVIRIS and 170 for ROSIS, while considering their spatial resolution and the memory footprint we established in this work. Hence, for the same spatial resolution, using the DD CASSI provides more spectral bands than the ROSIS sensor and fewer bands than the AVIRIS sensor. However, regardless of the sensor and thanks to acquisitions multiplexing, an improvement in sensor size would be made.

Since instead of having as many sensor rows as sensed spectral bands, it would only require as many rows as the required acquisitions. Thus, the sensor size would be divided by 5 or 10. Regarding the comparison between GPU and FPGA, since the limiting factor is data bandwidth, FPGAs have the upper hand thanks to their bigger work memory which reduces memory swapping.

## 5. REFERENCES

- [1] J. Aval, X. Briottet, S. Fabre, P.-Y. Foucher, V. Carrère, R. Marion, K. Uto, C. Weber, and M. Dalla Mura, "Applications in remote sensing – anthropogenic activities," in *Hyperspectral Imaging*, José Manuel Amigo, Ed., vol. 32 of *Data Handling in Science and Technology*, chapter 3.2, pp. 411–452. Elsevier, 2020.
- [2] T. Bajjouk, F. de Boissieu, J. Chanussot, S. Douté, M. Dumont, J.-B. Féret, T. Masson, A. Minghelli, P. Mouquet, F. Schmidt, and M. Dalla Mura, "Applications in remote sensing – natural landscapes," in *Hyperspectral Imaging*, José Manuel Amigo, Ed., vol. 32 of *Data Handling in Science and Technology*, chapter 3.1, pp. 371–410. Elsevier, 2020.
- [3] S.-E. Qian, *Hyperspectral satellites and system design*, CRC Press, 2020.
- [4] Planet, "Planet imagery product specifications," Tech. Rep., Planet Labs: San Francisco, CA, USA, 2022.
- [5] N. Hagen and M. W. Kudenov, "Review of snapshot spectral imaging technologies," *Optical Engineering*, vol. 52, no. 9, pp. 090901, sep 2013.
- [6] E. Candès and J. Romberg, "Sparsity and incoherence in compressive sampling," *Inverse Problems*, vol. 23, no. 3, pp. 969–985, Apr 2007.
- [7] A. Wagadarikar, R. John, R. Willett, and D. Brady, "Single disperser design for coded aperture snapshot spectral imaging," *Appl. Opt.*, vol. 47, no. 10, pp. B44–B51, Apr 2008.
- [8] M. E. Gehm, R. John, D. J. Brady, R. M. Willett, and T. J. Schulz, "Single-shot compressive spectral imaging with a dual-disperser architecture," *Opt. Express*, vol. 15, no. 21, pp. 14013–14027, Oct 2007.
- [9] L. Wang, Z. Xiong, D. Gao, G. Shi, and F. Wu, "Dual-camera design for coded aperture snapshot spectral imaging," *Appl. Opt.*, vol. 54, no. 4, pp. 848–858, Feb 2015.
- [10] J. Ramirez and H. Arguello, "Spectral image classification from multi-sensor compressive measurements," *IEEE Transactions on Geoscience and Remote Sensing*, vol. 58, no. 1, pp. 626–636, 2020.
- [11] M. Biquard, A. Rouxel, S. Lacroix, H. Carfantan, A. Monmayrant, and H. Camon, "Ccssnet: A learning algorithm for the segmentation of compressed hyperspectral images," in *2022 12th Workshop on Hyperspectral Imaging and Signal Processing: Evolution in Remote Sensing (WHISPERS)*, 2022, pp. 1–5.
- [12] N. Diaz, J. Ramirez, E. Vera, and H. Arguello, "Adaptive multisensor acquisition via spatial contextual information for compressive spectral image classification," *IEEE Journal of Selected Topics in Applied Earth Observations and Remote Sensing*, vol. 14, pp. 9254–9266, 2021.
- [13] I. García-Sánchez, O. Fresnedo, J. P. González-Coma, and L. Castedo, "Coded aperture hyperspectral image reconstruction," *Sensors*, vol. 21, no. 19, 2021.
- [14] X. Yuan, D. J. Brady, and A. K. Katsaggelos, "Snapshot compressive imaging: Theory, algorithms, and applications," *IEEE Signal Processing Magazine*, vol. 38, no. 2, pp. 65–88, 2021.
- [15] X. Miao, X. Yuan, Y. Pu, and V. Athitsos, "lambda-net: Reconstruct hyperspectral images from a snapshot measurement," in *2019 IEEE/CVF International Conference on Computer Vision (ICCV)*, 2019, pp. 4058–4068.
- [16] O. Ronneberger, P. Fischer, and T. Brox, "U-net: Convolutional networks for biomedical image segmentation," *CoRR*, vol. abs/1505.04597, 2015.
- [17] H. Zhang, I. Goodfellow, D. Metaxas, and A. Odena, "Self-attention generative adversarial networks," 2019.
- [18] S. Zhang, H. Huang, and Y. Fu, "Fast parallel implementation of dual-camera compressive hyperspectral imaging system," *IEEE Transactions on Circuits and Systems for Video Technology*, vol. 29, no. 11, pp. 3404–3414, 2019.
- [19] J. M. Bioucas-Dias and M. A. T. Figueiredo, "A new twist: Two-step iterative shrinkage/thresholding algorithms for image restoration," *IEEE Transactions on Image Processing*, vol. 16, no. 12, pp. 2992–3004, 2007.
- [20] S. Boyd, N. Parikh, E. Chu, B. Peleato, and J. Eckstein, *Distributed Optimization and Statistical Learning via the Alternating Direction Method of Multipliers*, Now Foundations and Trends, 2011.
- [21] O. Lim, S. Mancini, and M. Dalla Mura, "Feasibility of a real-time embedded hyperspectral compressive sensing imaging system," *Sensors*, vol. 22, no. 24, 2022.
- [22] M. Hanke, *Conjugate Gradient Type Methods for Ill-Posed Problems*, CRC Press, 2017.
- [23] I. Ardi, H. Carfantan, S. Lacroix, and A. Monmayrant, "Fast hyperspectral cube reconstruction for a double disperser imager," in *26th European Signal Processing Conference (EU-SIPCO 2018)*, Roma, Italy, Sep 2018.
- [24] NASA, "Avisir - airborne visible / infrared imaging spectrometer," <https://aviris.jpl.nasa.gov/index.html>.
- [25] Y. Saad, "Sparskit: a basic tool kit for sparse matrix computations," 1994.
- [26] S. Ayan, "Introduction to fixed point signal processing," <https://shafq.at/introduction-to-fixed-point-signal-processing.html>, 2020.
- [27] B. Kunkel, F. Blechinger, R. Lutz, R. Doerffer, H. van der Piepen, and M. Schroder, "ROSI (Reflective Optics System Imaging Spectrometer) - A Candidate Instrument For Polar Platform Missions," in *Optoelectronic Technologies for Remote Sensing from Space*, C. Stuart Bowyer and John S. Seeley, Eds. International Society for Optics and Photonics, 1988, vol. 0868, pp. 134 – 141, SPIE.
- [28] G. Lepage, J. Bogaerts, and G. Meynants, "Time-delay-integration architectures in cmos image sensors," *IEEE Transactions on Electron Devices*, vol. 56, no. 11, pp. 2524–2533, 2009.